

# Model-based Tensor Decompositions for Soil Moisture Estimation

Nikita Basargin<sup>a,b,c</sup>, Alberto Alonso-González<sup>d</sup>, and Irena Hajnsek<sup>a,e</sup>

<sup>a</sup>Microwaves and Radar Institute, German Aerospace Center (DLR), Weßling, Germany

<sup>b</sup>School of Life Sciences, Technical University of Munich (TUM), Freising, Germany

<sup>c</sup>Munich School for Data Science (MUDS), Munich, Germany

<sup>d</sup>Signal Theory and Communications Department (TSC), Universitat Politècnica de Catalunya (UPC), Barcelona, Spain

<sup>e</sup>Institute of Environmental Engineering, ETH Zürich, Zürich, Switzerland

## Abstract

Current and future SAR missions offer the potential to obtain high-resolution soil moisture estimates with large coverage and frequent revisit times. This work extends model-based polarimetric inversion methods from coherency matrices to tensors by integrating an additional spatial data dimension. The resulting data tensor is decomposed into model-based components by solving an optimization problem. Tensors offer a larger observation space in comparison to coherency matrices, allowing the use of more complex physical models that cover a more extensive range of scenarios. The proposed three-component decomposition characterizes image areas in terms of model-based scattering mechanisms. Physical parameters, including the soil dielectric constant, are directly obtained through optimization. The proposed method is extensible and is well suited for geophysical parameter estimation from increasingly available multidimensional SAR data.

## 1 Introduction

SAR sensors provide weather-independent and high-resolution images offering sensitivity to dielectric and geometrical properties. These properties make SAR an important data source for estimating a wide range of geophysical parameters. Soil moisture estimation from SAR data has been an active research topic with several works focusing on polarimetric [1], [2] and interferometric [3], [4] techniques.

One of the challenges is the presence of vegetation and the separation of the ground and vegetation scattering. Physical polarimetric models have been employed to decompose the polarimetric data into several components and estimate soil moisture from the components associated with the ground.

Since polarimetric data has a limited number of observables, the number of physical parameters that define the components and can be uniquely inverted is also limited. This restricts the complexity of applied models and can require hand-crafted inversion rules to resolve ambiguities if there are more model parameters than observables. For example, the inversion can include conditions to set specific parameters to a constant value based on the data properties. This work evaluates a new approach for model inversion inspired by tensor decompositions. To address the limited number of components, we propose to increase the observation space by additional data dimensions. With more observables, more complex physical models that describe the data more accurately can be employed and inverted.

Model inversion is formulated as an optimization problem. We iteratively adjust the model parameters to minimize the distance between the model prediction and the measured

data. After convergence, we obtain the physical parameters that best fit the data.

## 2 Methods

### 2.1 Tensor Decompositions

Tensor decompositions generalize matrix decompositions like eigendecomposition or SVD to higher-dimensional data. They directly operate on tensors and jointly process the information along all dimensions. There exist several tensor decomposition formulations, including the CP [5], [6] and Tucker [7] decompositions. In the CP decomposition, a tensor  $\mathcal{X}$  is approximated by a sum of components. Each component is an outer product of factor vectors, one factor for each tensor dimension. A three-dimensional tensor  $\mathcal{X} \in \mathbb{C}^{I \times J \times K}$  can be approximated by  $R$  components with factor vectors  $\mathbf{a}_r \in \mathbb{C}^I$ ,  $\mathbf{b}_r \in \mathbb{C}^J$ , and  $\mathbf{c}_r \in \mathbb{C}^K$ :

$$\mathcal{X} \approx \sum_{r=1}^R \mathbf{a}_r \circ \mathbf{b}_r \circ \mathbf{c}_r \quad (1)$$

where  $\circ$  represents the outer product.

### 2.2 Polarimetric Decompositions

Second-order polarimetric data is commonly represented with covariance or coherency matrices. Incoherent polarimetric model-based decompositions like Freeman–Durden [8] and Yamaguchi [9] approximate a single polarimetric coherency matrix by a sum of components. Each component is defined by a physical model associated with a specific scattering mechanism. Given a coherency matrix  $\mathbf{T} \in \mathbb{C}^{3 \times 3}$  in the Pauli basis, the Freeman–Durden decom-

position approximates it by three components:

$$\mathbf{T} = \mathbf{T}_s + \mathbf{T}_d + \mathbf{T}_v \quad (2)$$

where  $\mathbf{T}_s$ ,  $\mathbf{T}_d$ , and  $\mathbf{T}_v$  are the surface, dihedral, and volume scattering components, respectively.

The components are internally defined by a set of parameters. For example, the surface component in the Freeman–Durden decomposition has two parameters  $f_s$  and  $\beta$ :

$$\mathbf{T}_s = f_s \begin{bmatrix} 1 & \beta^* & 0 \\ \beta & |\beta|^2 & 0 \\ 0 & 0 & 0 \end{bmatrix} \quad (3)$$

There is a limit to the number of model parameters that can be uniquely inverted from a single coherency matrix. The matrix  $\mathbf{T}$  is Hermitian and has 9 independent real-valued observables: three real-valued diagonal elements and three complex-valued off-diagonal elements. Therefore, at most 9 physical parameters can be used to define the model components. Otherwise, the inversion is ambiguous. If the chosen physical model ignores some observables (e.g., assuming constant values or real-valued off-diagonal elements), the number of possible physical parameters is less than 9. For example, the Freeman–Durden decomposition assumes reflection symmetry (matrix elements  $\mathbf{T}_{[1,3]} = \mathbf{T}_{[2,3]} = 0$ ), resulting in 5 real-valued observables.

With a limited number of parameters, only relatively simple physical models can be inverted. This can result in cases where the model cannot accurately describe the data or has a small validity range.

### 2.3 Model-based Tensor Decomposition

To allow detailed models with more parameters, we combine the concepts of tensor decompositions and model-based polarimetric decompositions. Instead of inverting a single polarimetric coherency matrix, we extend the observation space and jointly invert multiple matrices stacked along a new dimension. Depending on the available data and physical model, the new data dimension can be, for example, spatial, temporal, or frequency. The stack of  $N$  polarimetric  $3 \times 3$  matrices forms a tensor  $\mathcal{X} \in \mathbb{C}^{N \times 3 \times 3}$  that is approximated by a sum of model-based components:

$$\mathcal{X} \approx \mathcal{R} = \sum_{r=1}^R \mathcal{C}_r \quad (4)$$

where  $\mathcal{R}$  is the reconstruction tensor approximating  $\mathcal{X}$  and  $\mathcal{C}_r$  are the component tensors.

Similarly to polarimetric model-based decompositions, each component is associated with a specific scattering mechanism defined by a set of parameters and a corresponding physical model. The details of the physical model depend on the new data dimension chosen to form the tensor. We discuss the use of the spatial dimension and models for soil moisture estimation in Section 2.5.

The use of a larger observation space allows to have more physical parameters that can be uniquely inverted. However, the number of parameters is still limited. Therefore, we share certain parameters across all coherency matrices

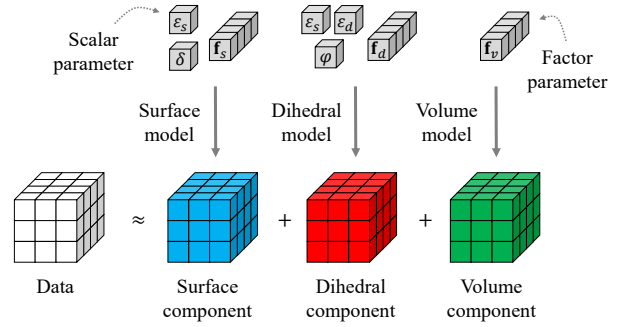


**Figure 1** Model-based Tensor Decomposition: A data tensor is approximated by a sum of model-based components. Each component is defined by a physical model that reconstructs the component from a set of parameters. Shared scalar parameters have the same value along the new data dimension. Factor parameters are represented by vectors and have different values along the new dimension.

and let other parameters vary along the new data dimension. The shared *scalar* parameters have the same value for each coherency matrix in the stack. In contrast, the *factor* parameters can have a different value for each matrix. We group the different values of a factor parameter into an  $N$ -element parameter vector that resembles a factor vector from the CP decomposition. The concept of scalar and factor parameters is illustrated in **Figure 1**.

### 2.4 Model Inversion with Optimization

The inversion of the physical parameters from the data can be performed in several ways. An analytical approach is computationally efficient but might be unavailable or difficult to derive for complex physical models. Therefore, a generic inversion approach that can handle different data dimensions and physical models is desirable.

We propose using numerical optimization to perform the decomposition and obtain the physical parameters. Optimization can be computationally expensive but offers more flexibility, allows additional constraints, and separates the decomposition design from the model inversion.

The physical models discussed in this work are differentiable mathematical functions. Therefore, methods based on gradient descent can iteratively solve the optimization problem. We start the inversion by initializing the physical parameters either randomly or at expected values (if available). In every iteration, we first apply the physical model to map the parameters to the component tensors  $\mathcal{C}_r$ . Then, the components are summed to obtain the reconstruction  $\mathcal{R}$ . In the next step, we measure the distance between  $\mathcal{R}$  and  $\mathcal{X}$  by evaluating a loss function  $l$ :

$$L = l(\mathcal{X}, \mathcal{R}) \quad (5)$$

The loss value  $L \in \mathbb{R}$  indicates how well  $\mathcal{R}$  reconstructs  $\mathcal{X}$ . To minimize  $L$  and obtain a good reconstruction, we compute the gradients of each physical parameter with respect to  $L$  using automatic differentiation. Then, we adjust the parameters based on the computed gradients using an

optimization algorithm, e.g., Adam [10]. The parameters can additionally be constrained to a physically valid value range depending on the model. This iterative process is repeated until convergence.

In recent years, excellent optimization frameworks have been developed. In our experiments, we use the PyTorch [11] framework to perform model-based tensor decomposition and obtain the physical parameters. The framework offers automatic differentiation, supports complex-valued tensors, and includes implementations of optimization algorithms. In addition, PyTorch can significantly reduce computational time by providing efficient library functions and GPU acceleration.

## 2.5 Soil Moisture Estimation

This section discusses an algorithm for soil moisture estimation based on the proposed model-based tensor decomposition. In this work, we restrict the decomposition to polarimetric data to reuse the existing physical models and compare the proposed approach to existing methods. The spatial domain is used as the additional data dimension to form tensors. This approach comes at the cost of reduced spatial resolution for the estimated parameters but increases the observation space, allowing the inversion of models with more parameters.

### 2.5.1 Tensor Formation

The tensors to be decomposed are formed using the coherency matrices obtained from a small spatial patch. First, the coherency matrices are estimated from fully polarimetric single-look complex (SLC) data. Since the matrix formation involves spatial averaging, the multilook windows must be non-overlapping to avoid redundancy between spatially adjacent matrices. Then, small spatial patches are chosen, and the coherency matrices within the patches are stacked into a tensor. In our experiments, we use spatial patches that contain  $N = 4 \times 4 = 16$  independent  $3 \times 3$  coherency matrices, resulting in a tensor  $\mathcal{X} \in \mathbb{C}^{16 \times 3 \times 3}$  for each spatial patch.

### 2.5.2 Physical Model

We use a three-component polarimetric model with surface, dihedral, and volume components to describe the data. The X-Bragg model proposed in [12] defines the surface component. Three parameters describe the surface scattering amplitude  $\mathbf{f}_s$ , the soil dielectric constant  $\varepsilon_s$ , and a term characterizing the soil roughness  $\delta$ . The dihedral component describes smooth double-bounce scattering and follows the model from [1]. Three additional parameters are required: the dihedral scattering amplitude  $\mathbf{f}_d$ , the trunk dielectric constant  $\varepsilon_d$ , and a differential propagation phase  $\phi$ . The volume component assumes randomly oriented dipole scattering and is equivalent to the volume component used in the Freeman-Durden decomposition. The only parameter is the volume scattering amplitude  $\mathbf{f}_v$ .

In total, this three-component model has 7 parameters:  $\mathbf{f}_s$ ,  $\mathbf{f}_d$ ,  $\mathbf{f}_v$ ,  $\varepsilon_s$ ,  $\varepsilon_d$ ,  $\delta$ , and  $\phi$ . However, it only describes three real-valued diagonal elements and one complex-valued off-diagonal element of the polarimetric coherency matrix (5

real-valued observables). Therefore, unique inversion is impossible with a single coherency matrix, and an extension to tensors is required.

Assumptions about the data must be made to extend the physical models designed for a single coherency matrix to a tensor formed from multiple matrices. Since the spatial dimension is used to form the tensor in this work, we can assume that certain parameters do not change significantly across the spatial patch. Those scalar parameters are shared across all coherency matrices in the tensor and have the same parameter value for each matrix during each reconstruction step. Other factor parameters are allowed to have different values for each matrix.

In our case, we allow the amplitude parameters  $\mathbf{f}_s$ ,  $\mathbf{f}_d$ , and  $\mathbf{f}_v$  to have individual values for each matrix along the spatial dimension. These parameters are represented by  $N$ -element factor vectors. The remaining parameters  $\varepsilon_s$ ,  $\varepsilon_d$ ,  $\delta$ , and  $\phi$  are shared and remain scalars. For a tensor formed from a stack of  $N$  matrices, we have  $5N$  useful observables and  $3N + 4$  model parameters.

Note that the model does not directly provide soil moisture estimates, instead providing the soil dielectric constant  $\varepsilon_s$ . The conversion from  $\varepsilon_s$  to the soil moisture is performed by applying a polynomial transformation from [13].

### 2.5.3 Loss Function

The loss function is an important metric that guides the optimization process toward the solution and indicates how well the model fits the data. A common choice also used in the CP decomposition is the L2 (or squared error) loss:

$$l(\mathcal{X}, \mathcal{R}) = \|\mathcal{X} - \mathcal{R}\|^2 \quad (6)$$

where  $\|\mathcal{Y}\|$  denotes the L2 norm of tensor  $\mathcal{Y} \in \mathbb{C}^{I_1 \times \dots \times I_N}$ :

$$\|\mathcal{Y}\| = \sqrt{\sum_{i_1=1}^{I_1} \sum_{i_2=1}^{I_2} \dots \sum_{i_N=1}^{I_N} |\mathcal{Y}_{[i_1, i_2, \dots, i_N]}|^2} \quad (7)$$

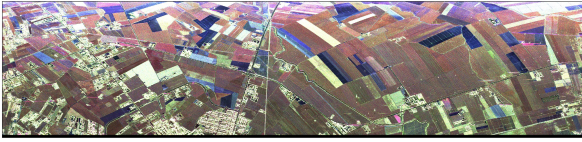
and  $\mathcal{Y}_{[i_1, i_2, \dots, i_N]}$  denotes the element of  $\mathcal{Y}$  found at index  $[i_1, i_2, \dots, i_N]$ .

The choice of the loss function makes implicit assumptions on the data distribution. For example, the L2 loss assumes that the data follows the Gaussian distribution [14]. The coherency matrices are Wishart-distributed, meaning that the L2 loss may not be the most appropriate function to measure similarity. However, compared to the Wishart loss, L2 is very efficient in terms of the computation cost and provides a simple and effective similarity measure. For this reason, we use the L2 loss in the following experiments.

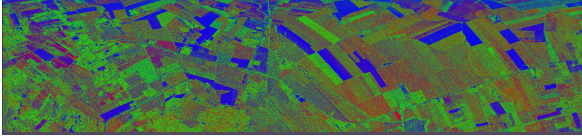
### 2.5.4 Validity Conditions

Solving an optimization problem iteratively always produces a solution. Therefore, all image patches can be inverted. However, for some areas, even complex models will not be able to fit the data well and may produce unreliable estimates. Therefore, some decomposition estimations should be discarded based on validity conditions that depend on the application.

In this work, we are primarily interested in the soil moisture estimates. We regard all patches as valid, where the



(a) Pauli RGB image: HH+VV, HH-VV, and HV+VH polarizations in blue, red, and green, respectively.



(b) Relative component powers indicate the relative intensity of model-based components: surface, dihedral, and volume scattering in blue, red, and green, respectively.

**Figure 2** The decomposition allows the characterization of different areas in terms of the model-based scattering mechanisms and their intensity.

surface dielectric estimate is in the validity range of the X-Bragg model:  $\epsilon_s \in [3, 25]$ . For invalid patches, the model cannot accurately describe the data, and the estimates are unreliable.

Another possibility to discard unreliable estimates is based on the loss function. Patches with a large loss value do not provide a reasonable reconstruction and can also be discarded.

### 3 Dataset

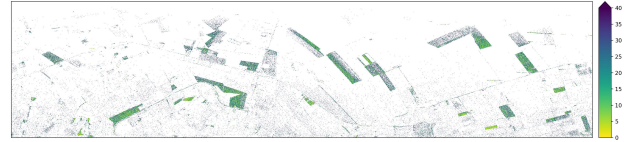
The dataset used to perform experiments was obtained by the DLR F-SAR [15] airborne radar during the HTERRA campaign in 2022 in the province of Foggia, Italy. The examined area covers many agricultural fields with different crop types, as shown in the Pauli RGB image in **Figure 2a**. A number of soil moisture ground measurements were obtained during the campaign. It should be noted that several fields are irrigated, and we expect to see both dry and wet areas. L-band data is used for the experiments and validation, motivated by the validity range of the X-Bragg model, which is larger for longer wavelengths.

F-SAR data is multi-looked to the resolution of approximately 3 meters in azimuth and range, which results in 11 independent looks per coherency matrix. Using  $4 \times 4$  spatial patches to form the tensors, we obtain soil moisture estimates at a resolution of 12 meters.

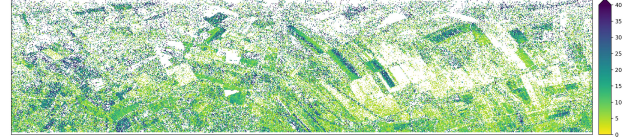
## 4 Experimental Results

### 4.1 Component Powers

After decomposing the tensors into components, we obtain three coherency matrices describing the surface, dihedral, and volume contributions for each resolution cell. This allows us to characterize each resolution cell regarding the dominant scattering mechanism. The characterization is somewhat similar to the characterization with the Freeman-



(a) Soil moisture estimation using only the X-Bragg surface component (method from [12])



(b) Soil moisture estimation using the model-based tensor decomposition

**Figure 3** Comparison of soil moisture estimates. The original X-Bragg method from [12] achieves a relatively low inversion rate. Three-component tensor decomposition is able to cover more scenarios by employing a more complex model.

Durden decomposition. The main difference is the use of more complex models for the surface and dihedral components. The component powers for each resolution cell are obtained by taking the trace of the obtained coherency matrices. Then, relative powers are obtained by dividing each power by the sum of powers.

**Figure 2b** shows the obtained relative component powers where each value in the range between 0 and 1 is directly translated into RGB color. The differences between fields are clearly visible: bare or slightly vegetated fields appear in blue (dominant surface scattering), while fields with taller or denser vegetation appear in red or green, indicating dominant dihedral or volume scattering, respectively.

### 4.2 Soil Moisture Inversion Rate

The advantage of using more complex models that can represent a larger range of scenarios is illustrated in **Figure 3**. An inversion using only a single X-Bragg surface component following the method from [12] is shown in **Figure 3a**. The inversion rate is relatively low, and soil moisture estimates can only be obtained for a few fields. In contrast, a significantly larger area can be inverted using the three-component model as shown in **Figure 3b**.

Similar conclusions have been presented in [2], where a similar three-component polarimetric model was also used, combined with a different inversion approach.

### 4.3 Estimation Validation

The quality of soil moisture estimation is mainly influenced by the employed physical model and depends on how well the model fits the data. **Figure 4** shows the estimated values plotted against ground measurements obtained over an almost bare field. We observe a clear correlation between the estimated and the measured values.

The estimations in densely vegetated areas with more complex scattering mechanisms are still challenging and do not obtain reliable soil moisture estimates with the current ap-

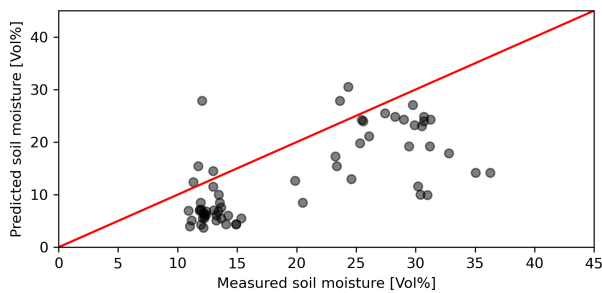


**Figure 4** Comparison of the measured and predicted soil moisture values over bare surfaces for the three-component model-based tensor decomposition.

proach. One reason is a simple volume scattering model that assumes randomly oriented dipoles. More complex models, for example, the parametric volume representation from [2], can be investigated in the future.

Another promising direction is the integration of different data dimensions like interferometry. While using the spatial domain allows us to invert more parameters uniquely, the information content may not be sufficient to separate the ground and volume contributions well. In contrast, interferometry adds sensitivity to the vertical distribution of scatterers and is very promising to improve the separation.

## 5 Conclusion

In this work, model-based decomposition techniques for polarimetric matrices have been extended to higher-order data tensors. This approach is promising since it jointly processes the information from a larger observation space and enables the use of more complex physical models that require more parameters. We demonstrate this by inverting a three-component model with more parameters than the classical PolSAR decomposition models like Freeman-Durden.

Soil moisture inversion using polarimetric and spatial information was presented. The obtained component powers directly indicate the type of the dominant scattering mechanism. Furthermore, the decomposition directly provides the physical parameters best fitting the observed data.

The quality of the estimation mainly depends on the employed physical model. Over bare surfaces, the obtained soil moisture estimates show a clear correlation to the ground measurements. Over densely vegetated areas where the employed model is not able to fit the data well, a larger reconstruction error is observed. These findings suggest the importance of a good model for the vegetation component. The integration of the spatial dimension increases the observation space and allows the inversion of more parameters at the cost of reduced resolution. It is important to keep in mind that the amount of additional information in the spatial dimension can be limited when all coherency matrices in the spatial patch are similar to each other. Therefore, the proposed model-based tensor decomposition can benefit from integrating additional data dimensions such as interferometry/tomography or multi-frequency data.

## 6 Literature

- [1] I. Hajnsek, T. Jagdhuber, H. Schon, and K. P. Papathanassiou, "Potential of estimating soil moisture under vegetation cover by means of PolSAR", *IEEE Transactions on Geoscience and Remote Sensing*, vol. 47, no. 2, pp. 442–454, 2009. DOI: 10.1109/TGRS.2008.2009642.
- [2] T. Jagdhuber, I. Hajnsek, and K. P. Papathanassiou, "An iterative generalized hybrid decomposition for soil moisture retrieval under vegetation cover using fully polarimetric SAR", *IEEE Journal of Selected Topics in Applied Earth Observations and Remote Sensing*, vol. 8, no. 8, pp. 3911–3922, 2014.
- [3] F. De Zan and G. Gomba, "Vegetation and soil moisture inversion from SAR closure phases: First experiments and results", *Remote Sensing of Environment*, vol. 217, pp. 562–572, 2018.
- [4] S. Zwieback, S. Hensley, and I. Hajnsek, "Soil moisture estimation using differential radar interferometry: Toward separating soil moisture and displacements", *IEEE Transactions on Geoscience and Remote Sensing*, vol. 55, no. 9, pp. 5069–5083, 2017.
- [5] J. D. Carroll and J.-J. Chang, "Analysis of individual differences in multidimensional scaling via an N-way generalization of "Eckart-Young" decomposition", *Psychometrika*, vol. 35, no. 3, pp. 283–319, 1970.
- [6] R. A. Harshman *et al.*, "Foundations of the PARAFAC procedure: Models and conditions for an "explanatory" multimodal factor analysis", 1970.
- [7] L. R. Tucker, "Some mathematical notes on three-mode factor analysis", *Psychometrika*, vol. 31, no. 3, pp. 279–311, 1966.
- [8] A. Freeman and S. L. Durden, "A three-component scattering model for polarimetric SAR data", *IEEE Transactions on Geoscience and Remote Sensing*, vol. 36, no. 3, pp. 963–973, 1998.
- [9] Y. Yamaguchi, T. Moriyama, M. Ishido, and H. Yamada, "Four-component scattering model for polarimetric SAR image decomposition", *IEEE Transactions on Geoscience and Remote Sensing*, vol. 43, no. 8, pp. 1699–1706, 2005.
- [10] D. P. Kingma and J. Ba, "Adam: A method for stochastic optimization", *arXiv preprint arXiv:1412.6980*, 2014.
- [11] A. Paszke, S. Gross, S. Chintala, *et al.*, *Automatic differentiation in PyTorch*, 2017.
- [12] I. Hajnsek, E. Pottier, and S. R. Cloude, "Inversion of surface parameters from polarimetric SAR", *IEEE Transactions on Geoscience and Remote Sensing*, vol. 41, no. 4, pp. 727–744, 2003.
- [13] G. C. Topp, J. Davis, and A. P. Annan, "Electromagnetic determination of soil water content: Measurements in coaxial transmission lines", *Water resources research*, vol. 16, no. 3, pp. 574–582, 1980.

- [14] D. Hong, T. G. Kolda, and J. A. Dersch, “Generalized canonical polyadic tensor decomposition”, *SIAM Review*, vol. 62, no. 1, pp. 133–163, 2020.
- [15] R. Horn, A. Nottensteiner, A. Reigber, J. Fischer, and R. Scheiber, “F-SAR - DLR’s new multifrequency polarimetric airborne SAR”, in *2009 IEEE International Geoscience and Remote Sensing Symposium*, IEEE, vol. 2, 2009, pp. II-902.